Design of a Dual-Band Quadrifilar Helix Antenna Using Stepped-Width Arms

Gangil Byun, Hosung Choo, and Sunwoo Kim

***Abstract*—This communication proposes the design of a quadrifilar helix antenna (QHA) with stepped-width arms and a meander feeding network. The stepped-width arms are applied to reduce the antenna size and adjust the frequency interval for dual-band operation. The feeding network includes a 90°-hybrid chip coupler and two meander lines that are designed to give a 180°-phase delay. The proposed QHA is optimized using a genetic algorithm (GA) and then fabricated to measure its performances in a full anechoic chamber. The results demonstrate that the proposed antenna is suitable to be used for dual-band global positioning system (GPS) applications.**

***Index Terms*—Global positioning system (GPS) antennas, helix antennas, quadrifilar helix antennas (QHAs).**

I. Introduction

A global positioning system (GPS) has become essential in many applications that provide reliable information on a real-time location for military, civil, and commercial purposes. Since the GPS tracks satellite signals transmitted over long distances through the ionospheric layer [1], GPS antennas are often required to provide circular polarization (CP) characteristics to minimize the ionospheric loss. In addition, these antennas need to have uniform pattern distributions over most of the upper hemisphere to maximize the coverage for the GPS satellites. For these reasons, a helix antenna has been a suitable candidate in many previous researches because of its broad CP bandwidth and high gain [2]–[4]. Its antenna characteristics can be further improved by applying quadrifilar arms with a sequential feeding network, which is known as a quadrifilar helix antenna (QHA) in [5]–[7]. Major achievements of previously reported QHAs are a reduction in antenna size by inserting ceramic rods, as Wang and Chung proposed [5], applying different pitch angles as Amin and Cahill suggested [6], and folding radiating arms reported by Chew and Saunders [7]; however, these methods often degrade the reception reliability of the system because of their narrow matching bandwidth and reduced gain. To maintain high reception reliability, dual-band characteristics have become an emerging design consideration in military GPS applications. Although the dual-band behavior can be achieved by applying multiple branches [8] and placing a coupled line parallel to existing helical arms [9], these approaches significantly increase the design complexity of QHAs, so more sophisticated work is requiring for miniaturized dual-band characteristics.

In this communication, we propose the design of a QHA using stepped-width arms with a quadrifilar feeding network that is composed of two meander lines and a printed circuit board (PCB). The stepped structure is adopted because of its simple impedance tuning characteristics that allow a reduction in antenna size and frequency interval adjustment for dual-band operations. Although the technique using the stepped impedance can be found in various microwave circuits that are mainly focused on their reflection and transmission characteristics, it has not been employed to achieve dual-band frequency responses for such radiating elements. To feed the arms with equal amplitudes and quadrature phases using a single 90°-hybrid chip coupler, two meander lines are added to our feeding network for an additional phase delay of 180°. This network is suitable because it minimizes the complexity of the PCB design and also lowers insertion losses of both transmission lines and couplers. To further improve the impedance matching characteristics and the radiation gain, detailed parameters are optimized using a genetic algorithm (GA) in conjunction with a full-wave electromagnetic (EM) simulator [10]. The optimized stepped-width arms and the meander lines are fabricated on a thin PET substrate, and antenna performances, such as reflection coefficients and radiation gains, are measured in a full anechoic chamber. The results prove that the stepped-width arms are suitable for size reduction and frequency interval adjustment for dual-band operation.

Manuscript received March 08, 2014; revised December 19, 2014; accepted January 18, 2015. Date of publication January 30, 2015; date of current version April 03, 2015. This work was supported in part by Civil Military Technology Cooperation (CMTC) and in part by the Basic Science Research Program through the National Research Foundation of Korea (NRF) funded by the Ministry of Education (NRF—2014R1A1A2055813).

G. Byun and S. Kim are with the Department of Electronics and Computer Engineering, Hanyang University, Seoul 133-791, South Korea (e-mail: remero@hanyang.ac.kr).

H. Choo is with the School of Electronic and Electrical Engineering, Hongik University, Seoul 121-791, South Korea (e-mail: hschoo@hongik.ac.kr).

Digital Object Identifier 10.1109/TAP.2015.2398463

II. Proposed Antenna Structure

A. Design Approach

Fig. 1 shows an unwrapped single arm that describes our design approach to the proposed QHA. The total length is designed to be about a half wavelength at around 1 GHz and is divided into four steps having widths of w_{m1}, w_{m2}, w_{m3}, and w_{m4} and lengths of l_{m1}, l_{m2}, l_{m3}, and l_{m4}, respectively. In our approach, the input impedance of the arm is adjusted by applying size variations between the steps. To verify the impedance tuning characteristics, only w_{m1} and w_{m3} are varied from 7.5 to 15 mm, and the other parameters are fixed as listed in Table I.

Fig. 2(a) shows reflection coefficients of the unwrapped arm according to w_{m1}, when w_{m3} is fixed at 7.5 mm. The figure illustrates that both resonances shift toward the lower frequency band, as the size of the upper step becomes larger. Fig. 2(b) exhibits the effect of the size variation in the middle step that is specified by parameter w_{m3}, while w_{m1} is fixed at 7.5 mm. The result demonstrates that higher resonant frequency can be independently adjusted by w_{m3}, which results in a reduced frequency interval between the two resonances. Thus, in our proposed QHA, the stepped-width arm is adopted to realize dual-band operation with a reduced antenna size in the GPS L1 and L2 bands.

B. Proposed Antenna Design

Fig. 3(a) shows a side view of the proposed antenna that consists of four helical arms, from h_2 to h_1, and a feeding network. The feeding network includes two meander lines (meander 1 at h_3 and meander 2 at h_4) and a hybrid chip coupler (XC1400P-03S, Anaren [11]), which is attached to the PCB to feed the arms with equal amplitudes and has a phase difference of 90°. Since the single chip coupler is used in the feeding network, the antenna can have a simple PCB design and low transmission line losses. Fig. 3(b) shows the top view of the antenna. As can be seen, the radiator is wrapped in a cylinder, which has a diameter of d_1, and the two meander lines are placed between the radiator and the PCB having a diameter of d_2. The diameter d_1 is determined to be about a quarter wavelength at 1.57542 GHz, and the

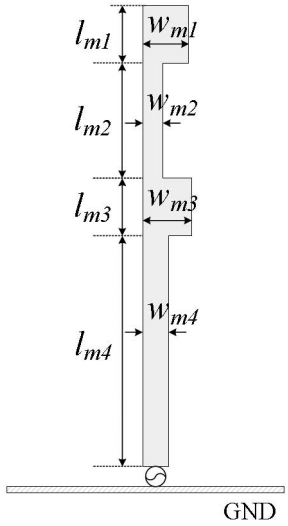

Fig. 1. Geometry of an unwrapped single arm.

TABLE I
PARAMETERS OF THE SINGLE ARM

Parameter	l_{m1}	l_{m2}	l_{m3}	l_{m4}	w_{m2}	w_{m4}
Value (mm)	24	38	24	67	5.5	

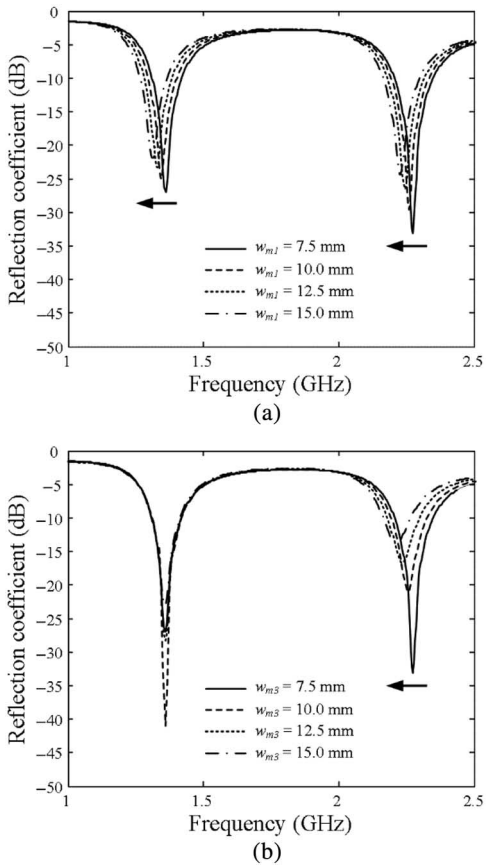

Fig. 2. Reflection coefficients of the single arm. (a) Effects of w_{m1}. (b) Effects of w_{m3}.

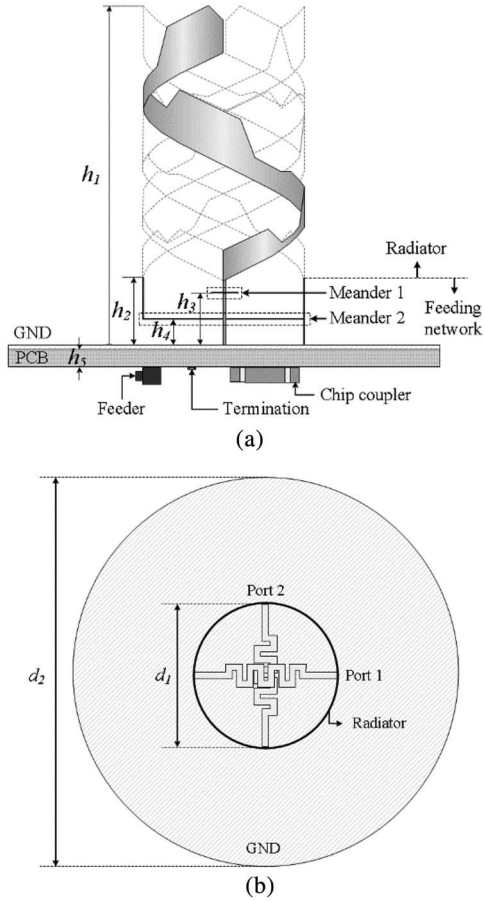

Fig. 3. Geometry of the proposed QHA. (a) Side view. (b) Top view.

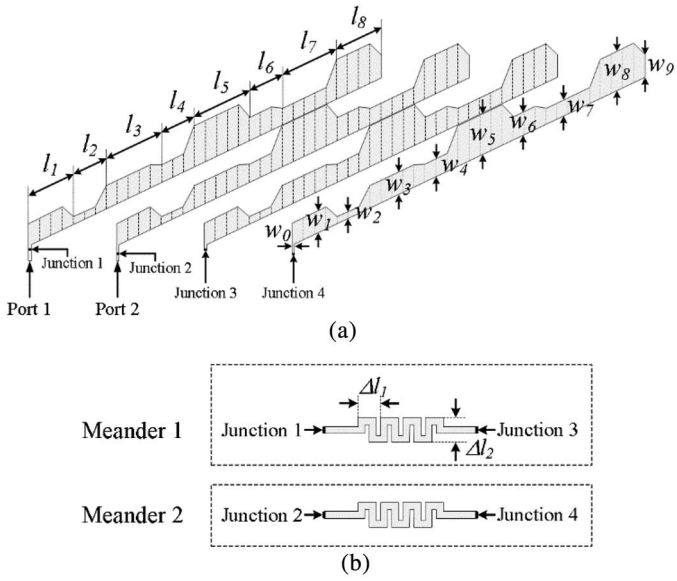

Fig. 4. Design layout of the proposed QHA. (a) Stepped arms. (b) Meander lines.

diameter d_2 is designed to be about a half wavelength at 1.2276 GHz to maintain high front-to-back ratio of greater than 20 dB. Fig. 4(a) and (b) shows the design layouts of the stepped-width arms and the meander lines. The total length of each arm is designed to be about half

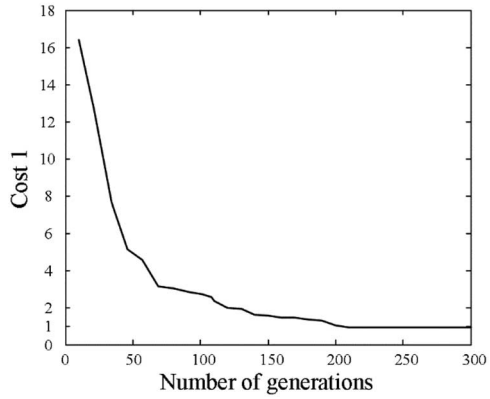

Fig. 5. Behavior of the cost function.

TABLE II
PARAMETERS OF THE OPTIMIZED ANTENNA

Parameter		Value (mm)
Helix widths	w_0	1.7
	w_1	8.1
	w_2	2.5
	w_3	8.4
	w_4	6.5
	w_5	15.3
	w_6	8.6
	w_7	5.9
	w_8	15.0
	w_9	8.9
Helix lengths	l_1	19.2
	l_2	14.4
	l_3	24.0
	l_4	14.4
	l_5	24.0
	l_6	14.4
	l_7	24.0
	l_8	19.2
Helix heights	h_1	81.6
	h_2	5.8
	h_3	3.4
	h_4	2.6
	h_5	1.0
Meander lengths	Δl_1	6.8
	Δl_2	6.7
Diameters	d_1	44.7
	d_2	120.0

a wavelength in the GPS L2 band, and the stepped-width variations are adjusted by applying different step widths ($w_1, w_2, \ldots, w_9$) from 0.5 to 15 mm with different step lengths ($l_1, l_2, \ldots, l_8$) to obtain dual resonances at the two target frequencies. We increased the number of steps for fine tuning to more improve the antenna performance and to further reduce the antenna size. As discussed in Section II-A, this stepped-width arm is implemented to adjust the input impedance of the radiating elements, so that the two resonances can be applied for the GPS L1 and L2 bands. For a quadrature phase excitation, the first and the second arms are linked to the two ports of the coupler, and the third and the fourth arms are connected to the first and the second arms through meander 1 and meander 2, respectively. The lengths of

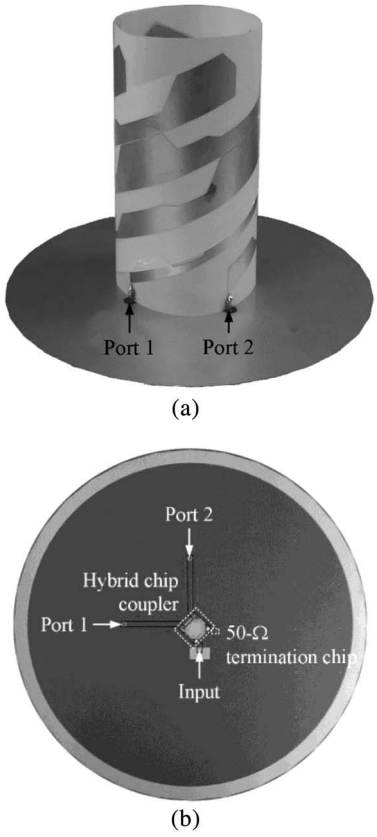

Fig. 6. Optimized antenna structure. (a) Photograph of the fabricated antenna. (b) Photograph of the PCB.

the meander lines (Δl_1 and Δl_2) are about a half wavelength at around 1.5 GHz to give a phase delay of 180°.

To further improve the radiation gain as well as the CP characteristics, the proposed antenna structure is optimized using the GA in conjunction with the FEKO EM simulator [12]. Equation (1) shows a cost function used in our optimization to raise the average CP gain of the antenna. G_{L1} and G_{L2} are the CP gains in the upper hemisphere ($0^\circ < \theta < 90^\circ$) at 1.57542 GHz (L1) and 1.2276 GHz (L2). N_ϕ and N_θ represent the number of points along ϕ- and θ-directions, respectively

$$\text{Cost1} = \frac{1}{\frac{1}{2}\left(\frac{1}{N_\phi N_\theta}\sum_{N_\theta}\sum_{N_\phi} G_{L1}(\phi,\theta) + \frac{1}{N_\phi N_\theta}\sum_{N_\theta}\sum_{N_\phi} G_{L2}(\phi,\theta)\right)}. \tag{1}$$

The convergence criteria of our optimization process is to achieve an average CP gain of greater than 0 dBic in the upper hemisphere, which implies that the cost value should be lower than "1" for convergence [13]. Fig. 5 exhibits the behavior of our cost function according to the number of generations and shows that the initial cost value of "16.41" was reduced by about one third at 46th generation with the value of "5.15." Our process took 210 generations to obtain the cost value of "0.91," and we presented its detailed design parameters in Table II. As observed in Section II-A, the antenna has two wide stepped-widths at the top and the middle of the arms. The length of the helical arms is optimized to be slightly smaller than half of a wavelength in the GPS L2 band, and the length of the meander lines is also about a half wavelength in the GPS L1 band.

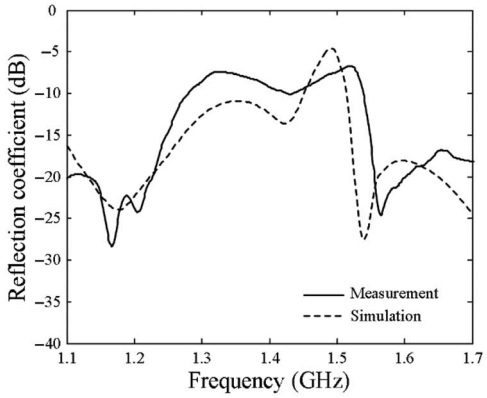

Fig. 7. Reflection coefficients.

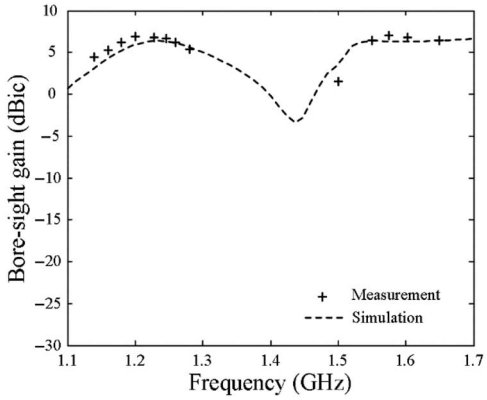

Fig. 8. Bore-sight gain.

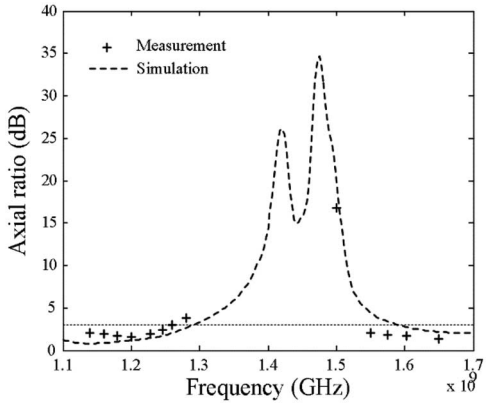

Fig. 9. Axial ratio.

III. Measurement and Analysis

To verify the antenna performances, such as reflection coefficients, bore-sight gain, axial ratio, and radiation patterns, the optimized helical arms and the meander lines are fabricated on a thin PET substrate ($\varepsilon_r = 2.3$, $\tan\delta = 0.022$) and assembled with the PCB, as shown in the Fig. 6(a) and (b). Fig. 7 presents the simulated reflection coefficients in comparison with the measurement. As can be seen, the antenna is well matched in the GPS L1 and L2 bands with the measured values of $-18.8\,s$ and -19.6 dB at 1.57542 and 1.2276 GHz, respectively. Radiation characteristics, such as gain, axial ratio, and patterns, are measured in a full anechoic chamber ($15.2\,\mathrm{m}\ (W)\ \times 7.9\,\mathrm{m}\ (L)\ \times 7.9\,\mathrm{m}\ (H)$), where the maximum number of frequency points is limited to 15 for scanning intervals of 5° in both ϕ- and θ-directions ($\mathrm{scanning\ speed} = 10^\circ/s$). Fig. 8 shows the bore-sight gain of the antenna as a function of frequency. The simulated data are

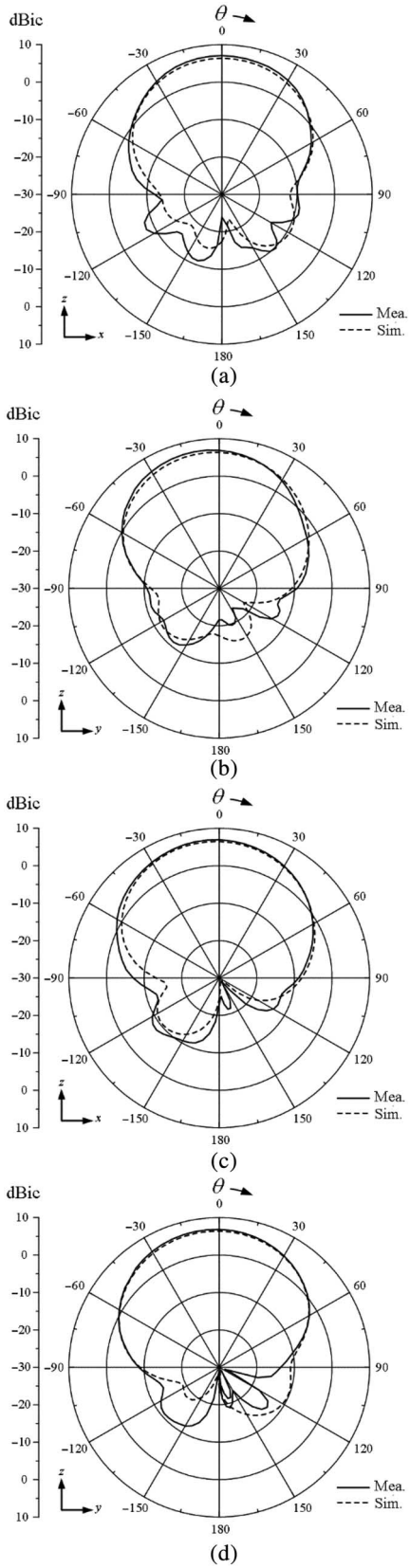

Fig. 10. Radiation patterns. (a) *zx*-plane at 1.57542 GHz. (b) *zy*-plane at 1.57542 GHz. (c) *zx*-plane at 1.2276 GHz. (d) *zy*-plane at 1.2276 GHz.

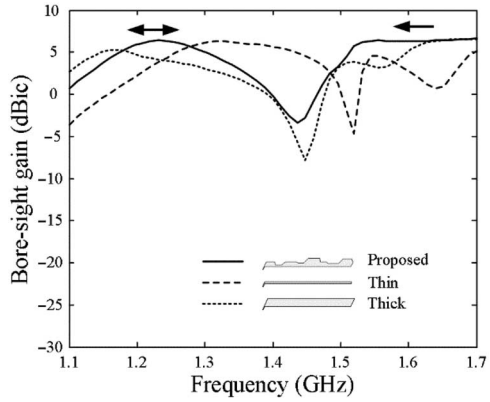

Fig. 11. Effect of stepped-width arms.

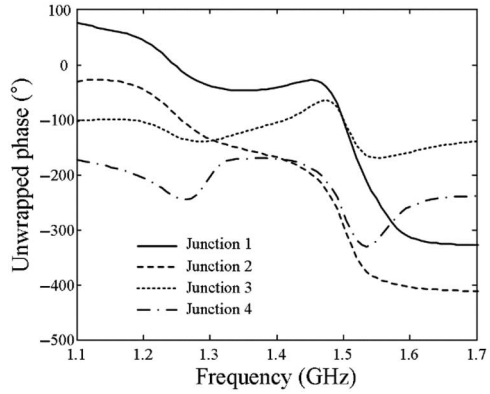

Fig. 12. Phase excitations to junctions.

presented by dashed lines and are compared with the measured data specified by "+" marks. As can be seen, both results show a good agreement with the measured values of 6.4 and 6.3 dBic at 1.57542 and 1.2276 GHz, respectively.

Fig. 9 shows the measured axial ratio in comparison with the simulation, which exhibits that the antenna has CP properties for dual-band operation with the axial ratio values of lower than 3 dB. The feeding network of the proposed antenna was further evaluated by applying amplitude and phase imbalances up to 3 dB and 50°, respectively, and we verified that both the axial ratio and the gain of the antenna were insensitive to those imbalances. For example, bore-sight gains were slightly degraded by 0.3 dB due to the amplitude imbalance and 0.6 dB in the presence of the phase imbalance.

Fig. 10(a) and (b) shows 2-D patterns in the *zx*- and *zy*-planes at 1.5754 GHz, and their half power beam widths (HPBWs) are 73.6° and 74.8°, respectively. Fig. 10(c) and (d) shows the patterns in the *zx*- and *zy*-planes at 1.2276 GHz with HPBWs of 79.9° and 80°, respectively.

To observe the effects of the stepped-width arms, the bore-sight gain of the proposed antenna is compared with that of both narrow (2.5 mm) and wide (15.3 mm) arms with no step variations. Fig. 11 presents gain-frequency responses of the three arm shapes connected to the same feeding network. As discussed in Section II-A, the stepped-width arms reduce the frequency interval between the two resonances from 516 (no step variations) to 348 MHz (stepped widths). Fig. 12 shows the current phases induced at the meander junctions to observe phase differences delivered from the proposed feeding network. As can be seen, the phase differences between the junctions are roughly 90° in both lower and higher frequency bands.

IV. Conclusion

We described the design of dual-band QHAs using stepped-width arms that are employed to reduce the antenna size and to adjust the frequency interval between two resonances for dual-band operation. To realize the quadrifilar feeding network, a 90°-hybrid chip coupler was fabricated on the PCB, and its two ports were connected to the meander lines that were designed to give a 180°-phase delay. To verify the suitability of the antenna, the stepped-width arms and the meander lines were fabricated on a thin PET substrate, and antenna performances, such as reflection coefficients and radiation gains, were measured in a full anechoic chamber. The results demonstrated that the proposed antenna is suitable for size reduction and dual-band CP operation with no significant degradation in radiation gain and patterns.

References

[1] A. T. Adams, R. K. Greenough, R. F. Wallenberg, A. Mendelovicz, and C. Lumjiak, "The quadrifilar helix antenna," *IEEE Trans. Antennas Propag.*, vol. 22, no. 2, pp. 173–178, Mar. 1974.

[2] J. M. Tranquilla and S. R. Best, "A study of the quadrifilar helix antenna for global positioning system (GPS) applications," *IEEE Trans. Antennas Propag.*, vol. 38, no. 10, pp. 1545–1550, Oct. 1990.

[3] D. K. C. Chew and S. R. Saunders, "Meander line technique for size reduction of quadrifilar helix antenna," *IEEE Antennas Wireless Propag. Lett.*, vol. 1, no. 1, pp. 109–111, Feb. 2005.

[4] S. Hebib, N. J. G. Fonseca, and H. Aubert, "Compact printed quadrifilar helical antenna with iso-flux-shaped pattern and high cross-polarization discrimination," *IEEE Antennas Wireless Propag. Lett.*, vol. 10, pp. 635–638, Jul. 2011.

[5] Y.-S. Wang and S.-J. Chung, "A miniature quadrifilar helix antenna for global positioning satellite reception," *IEEE Trans. Antennas Propag.*, vol. 57, no. 12, pp. 3746–3751, Dec. 2009.

[6] M. Amin and R. Cahill, "Effect of helix turn angle on the performance of a half wavelength quadrifilar antenna," *IEEE Microw. Wireless Compon. Lett.*, vol. 16, no. 6, pp. 384–386, Jun. 2006.

[7] J. Rabemanantsoa and A. Sharaiha, "Size reduced multi-band printed quadrifilar helical antenna," *IEEE Trans. Antennas Propag.*, vol. 59, no. 9, pp. 3138–3143, Sep. 2011.

[8] Y. Letestu and A. Sharaiha, "Broadband folded printed quadrifilar helical antenna," *IEEE Trans. Antennas Propag.*, vol. 54, no. 5, pp. 1600–1604, May 2006.

[9] Y. W. Chow, E. K. N. Yung, and H. T. Hui, "Quadrifilar helix antenna with parasitic helical strips," *Microw. Opt. Tech. Lett.*, vol. 30, no. 2, pp. 128–130, Jul. 2001.

[10] Y. Rahmat-Samii and E. Michielssen, *Electromagnetic Optimization by Genetic Algorithms*. Hoboken, NJ, USA: Wiley, 1999.

[11] *Hybrid Coupler Model: XC1400P-03S, Anaren* [Online]. Available: https://www.anaren.com/sites/default/files/XC1400P-03%20Data%20Sheet%20Rev%20C.pdf, accessed on 2012.

[12] EM Software and Systems. (2012). *FEKO Suite 6.1* [Online]. Available: http://www.feko.info

[13] R. Azaro, F. G. B. De Natale, M. Donelli, A. Massa, and E. Zeni, "Optimized design of a multifunction/multiband antenna for automotive rescue systems," *IEEE Trans. Antennas Propag.*, vol. 54, no. 2, pp. 392–400, Feb. 2006.